# Left-hand cut and the HAL QCD method

**Sinya Aoki,**[a,*] **Takumi Doi**[b] **and Yan Lyu**[b]

[a]*Center for Gravitational Physics and Quantum Information, Yukawa Institute for Theoretical Physics, Kyoto University, Kyoto 606-8502, Japan*

[b]*Interdisciplinary Theoretical and Mathematical Physics Program (iTHEMS), RIKEN, Wako 351-0198, Japan*

*E-mail:* saoki@yukawa.kyoto-u.ac.jp, doi@ribf.riken.jp, yan.lyu@riken.jp

We investigate how the left-hand cut (LHC) problem is treated in the HAL QCD method. For this purpose, we first consider the effect of the LHC to the scattering problem in non-relativistic quantum mechanics with potentials. We show that the $S$-matrix or the scattering phase shift obtained from the potential including the Yukawa term ($e^{-m_\pi r}/r$) with the infra-red (IR) cutoff $R$ is well-defined even for the complex momentum $k$ as long as $R$ is finite, and they are compared with those obtained by the analytic continuation without the IR cutoff. In the $R \to \infty$ limit, the phase shift approaches the result from the analytic continuation at $\mathrm{Im}\, k < m_\pi/2$, while they differ at $\mathrm{Im}\, k > m_\pi/2$, except $k = k_b$, where $k_b$ is the binding momentum. We also observe that $k_b$ can be correctly obtained even at finite but large $R$. Using knowledge obtained in the non-relativistic quantum mechanics, we present how we should treat the LHC in the HAL QCD potential method.

---

*Speaker

## 1. Introduction

The LHCb collaboration reported an experimental observation of a doubly charmed tetraquark state $T_{cc}^+$[1, 2], which appears around 360 keV below $D^{*+}D^0$ threshold as a narrow peak with $I(J^P) = 0(1^+)$ in the $D^0D^0\pi^+$ invariant mass spectrum, and thus is supposed to contain two charm quarks and two light anti-quarks. Therefore $T_{cc}^+$ is a genuine tetraquark state, since it cannot mix with an ordinary meson made of quark and anti-quark due to a conservation of a charm number.

Studies on the $T_{cc}^+$ state in lattice QCD is summarized in Fig. 1(Left), where the inverse scattering length $1/a_0$ for the $S$-wave $D^*D$ system in the $I = 0$ channel is plotted as a function of $m_\pi^2$. These data are extrapolated to $m_\pi = 135$ MeV linearly in $m_\pi^2$, leading to $1/a_0$ = -0.01(9) [fm$^{-1}$], which is consistent with $1/a_0$ = -0.03(4) [fm$^{-1}$] (black plus), obtained from the potential extrapolated to $m_\pi = 135$ MeV[6]. Thus $T_{cc}^+$ seems to appear as a very shallow (quasi) bound state of $D^*D$ at the physical pion mass.
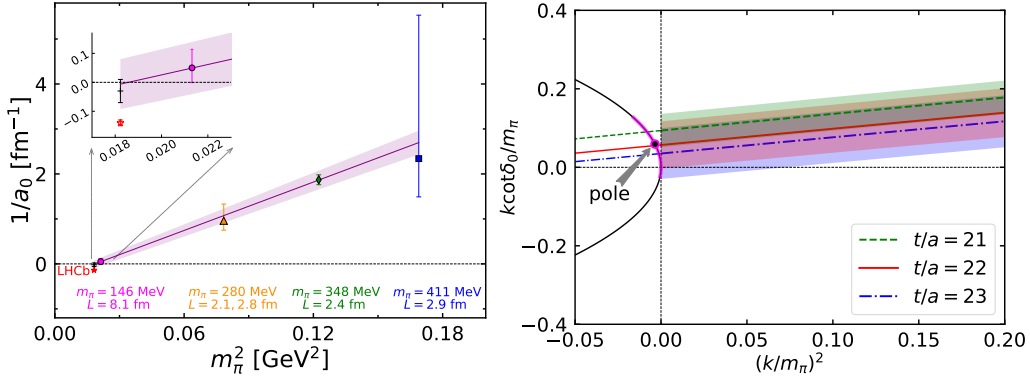


**Figure 1:** (Left) The inverse scattering length $1/a_0$ for the $S$-wave $D^*D$ system with $I = 0$ as a function of $m_\pi^2$, obtained from lattice QCD calculations by Refs. [3] (blue square), [4](green diamond), [5](yellow triangle), and [6](magenta circle), together with its chiral extrapolation of $1/a_0$ linear in $m_\pi^2$ (violet solid line). The black plus shows the value obtained from the potential extrapolated to $m_\pi = 135$ MeV[6], while the red star is the real part of the experimental value by LHCb[2]. (Right) The $k \cot \delta_0/m_\pi$ as a function of $(k/m_\pi)^2$, where $\delta_0$ is the $S$-wave phase shift of the $D^*D$ scattering in the $I = 0$. Its intersection with $\sqrt{-(k/m_\pi)^2}$ (the upper black solid line) gives the position of the virtual pole. Both figures are taken from [6].

However, it has been pointed out that the analysis in some lattice studies to obtain the scattering length in Fig. 1 may not be justified due to the presence of the left-hand cut (LHC)[7]. For example, in Ref. [5], the effective range expansion (ERE) was employed to obtain the scattering length from the finite volume energies, some of which, however, are out of the range for the ERE to be valid. To overcome difficulties associated with the LHC, analyses based on effective theories[7–9] as well as a modified finite volume formula in the presence of the LHC[10] have been proposed.

Does the LHC also affect the result in Ref. [6] using the HAL QCD method ? Fortunately, the virtual pole obtained in Ref. [6] appears above the branch point of the LHC, as shown in Fig. 1 (Right), where the LHC appears below $(k/m_\pi)^2 \simeq -0.02$. Therefore the analysis in [6] is unaffected by the LHC and thus valid. We however think that we need to understand what happens if a bound state appears on the LHC in the HAL QCD method for future studies.

## 2. Bound state on LHC

### 2.1 Left-hand cut

We show how the LHC appears in the $D^*D$ scattering. The virtual pion propagator in the $u$ channel scattering in the center of mass reads

$$\frac{1}{(E_{D^*} - E_D)^2 - (\vec{q} - \vec{p})^2 - m_\pi^2} = \frac{1}{m_{D^*}^2 + m_D^2 - m_\pi^2 - 2E_{D^*}E_D + 2k^2 \cos\theta}, \quad (1)$$

where $E_{D^*} = \sqrt{m_{D^*}^2 + k^2}$ and $E_D = \sqrt{m_D^2 + k^2}$ with $k := |\vec{q}| = |\vec{p}|$, and $\vec{q} \cdot \vec{p} = k^2 \cos\theta$. After the $S$ wave projection, the $u$ channel contribution is proportional to

$$\propto \frac{1}{k^2} \log \left[ \frac{m_{D^*}^2 + m_D^2 - m_\pi^2 - 2E_{D^*}E_D + 2k^2}{m_{D^*}^2 + m_D^2 - m_\pi^2 - 2E_{D^*}E_D - 2k^2} \right], \quad (2)$$

which generates two branch points at

$$k_\pm^2 = \frac{[(m_{D^*} - m_D)^2 - m_\pi^2][(m_{D^*} + m_D)^2 - m_\pi^2]}{4A_\pm}, \quad A_+ = m_\pi^2 \ll A_- = 2(m_{D^*}^2 + m_D^2) - m_\pi^2. \quad (3)$$

Therefore, if $(m_{D^*} - m_D)^2 - m_\pi^2 < 0$, there appears a cut at negative $k^2$, that is the left-hand cut.

### 2.2 LHC in the potential

In this subsection, we discuss that the LHC problem appears also in quantum mechanics. For the spherically symmetric potential, the $S$-wave Schrödinger equation reduces to

$$\left[ \frac{d^2}{dr^2} - U(r) + k^2 \right] \varphi(k, r) = 0, \quad (4)$$

where $k$ is related to the energy as $k^2 = 2ME$. For example, in the case of the Yukawa potential, we have

$$U(r) = g \frac{e^{-m_\pi r}}{r}, \quad (5)$$

which mimics the non–relativistic contribution of the virtual pion exchange with its mass $m_\pi$.

The $S$-matrix is defined as $S(k) = a/b$, where $a, b$ are determined from the asymptotic behavior of the regular solution satisfying $\varphi(k, 0) = 0$ and $\frac{d}{dr}\varphi(k, 0) = 1$ as

$$\varphi(k, r) \xrightarrow{r \to \infty} ae^{ikr} - be^{-ikr}. \quad (6)$$

The regular solution is explicitly given by

$$\varphi(k, r) = \frac{1}{2ik} \left[ e^{ikr} \mathcal{F}(-k, r) - e^{-ikr} \mathcal{F}(k, r) \right], \quad \mathcal{F}(k, r) = 1 + \int_0^r dr' e^{ikr'} U(r') \varphi(k, r'). \quad (7)$$

Therefore, if $U(r)$ has the IR cutoff $R$ as $U(r > R) = 0$, $S(k)$ is well-defined for $^\forall k \in \mathbb{C}$ as

$$S(k) = \frac{\mathcal{F}(-k, \infty)}{\mathcal{F}(k, \infty)} = \frac{\mathcal{F}(-k, R)}{\mathcal{F}(k, R)} := S(k, R), \quad (8)$$

so that there appears no LHC in $S(k, R)$. Since $U(r > R) = 0$ is physically a good approximation for $R \gg 1/m$, the LHC problem is rather academic. In other words, we may say who cares the tail of the potential behind the moon. Nonetheless, for the academic nature of the problem, we investigate how $S(k, R)$ in the large $R$ limit is different from an analytic continuation of $S_{\text{anal}}(k)$, obtained by the analytic continuation at $k^2 \geq 0$ of the $S$-matrix without IR cutoff.

### 2.3 Large $R$ limit

In the upper $k$ plane (Im $k \geq 0$ ) , $\mathcal{F}(k, R)$ is convergent as $R \to \infty$, while

$$
\begin{aligned}
\mathcal{F}(-k, R) &= 1 + \int_0^R dr'\, e^{-ikr'} U(r')\varphi(k, r') = \mathcal{F}(-k, \bar{R}) + \int_{\bar{R}}^R dr'\, e^{-ikr'} U(r')\varphi(k, r') \\
&\simeq \mathcal{F}(-k, \bar{R}) - g\frac{\mathcal{F}(k, \infty)}{2ik} \int_{\bar{R}}^R dr'\, e^{-i2kr'} \frac{e^{-m_\pi r'}}{r'},
\end{aligned} \tag{9}
$$

as $R \to \infty$, where we use

$$
\varphi(k, r) \simeq -\frac{\mathcal{F}(k, \infty)}{2ik} e^{-ikr} \tag{10}
$$

at large $r$ for Im $k \geq 0$. Since the integrand in the second term of Eq. (9) contains $e^{(2\mathrm{Im}k - m_\pi)r'}$, $\mathcal{F}(-k, R)$ is divergent (convergent) for Im$k > m_\pi/2$ ( Im$k < m_\pi/2$ ) as $R \to \infty$.

If there appears a bound state at $k = k_b$ for Im $k_b > 0$ as a pole of the $S$-matrix $S(k) = \mathcal{F}(-k, \infty)/\mathcal{F}(k, \infty)$, it implies $\mathcal{F}(k, \infty) = 0$. Therefore, according to (9), $\mathcal{F}(-k_b, R)$ is convergent even if Im $k_b > m_\pi/2$. Furthermore, at finite $R$, $S(k, R)$ has a pole at $k = k_b(R)$, which is $R$-dependent in principle, and it converges to $k_b$ as $\lim_{R \to \infty} k_b(R) = k_b$. Thus, $S(k_b(R), R)$ diverges even at finite $R$.

In summary, in the $R \to \infty$ limit, $S(k, R)$ is convergent at Im $k < m_\pi/2$, while $S(k, R)$ is divergent at Im $k > m_\pi/2$ due to the divergence of $\mathcal{F}(-k, \infty)$ except $k = k_b$. Moreover, $S(k_b(R), R)$ has a pole due to $\mathcal{F}(k_b(R), R) = 0$ event at finite $R$, and the pole converges to $k_b$ as $R \to \infty$.

### 2.4 Example: Yukawa plus Gaussian at short distance

As an explicit example, we consider a potential containing the Yukawa term (long range) plus a Gaussian term (short range). Parameters in the potential are adjusted so that one bound state appears below the branch point of the LHC. The scattering phase shift is calculated for $k^2 > 0$, and it is analytically continued to $k^2 < 0$ region. We also introduce the IR cutoff $R$ to the Yukawa part of the potential, and calculate the $S$-wave scattering phase shift $\delta_R(k)$ at $k^2 < 0$, using

$$
k \cot \delta_R(k) = ik\frac{S(k, R) + 1}{S(k, R) - 1}, \quad S(k, R) = \frac{\mathcal{F}(-k, R)}{\mathcal{F}(k, R)}, \tag{11}
$$

where both $\mathcal{F}(k, R)$ and $\mathcal{F}(-k, R)$ are convergent for the finite $R$.

We compare $k \cot \delta(k)$ obtained from the analytic continuation $S_{\mathrm{anal}}(k)$ with the result obtained from Eq. (11) for various values of $R$. In Fig. 2 (Left), $k \cot \delta(k)/m_\pi$ from the analytic continuation is plotted by the black symbols, while $k \cot \delta_R(k)/m_\pi$ obtained from Eq. (11) are given for $R = 5$ fm (green), 10 fm (blue), 15 fm (red), 20 fm (violet) and 25 fm (magenta), where we take $m_\pi = 146$ MeV. These EREs intersect with the bound state condition $-\sqrt{-(k/m_\pi)^2}$ (black dashed line) at $k_b = k_b(\infty)$ and $k_b(R)$. It is noted that $R$ dependence of $k_b(R)$ is very very small in this range of $R$, so that we regard $k_b = k_b(R)$ hereafter.

When Im $k < m_\pi/2$, $k \cot \delta_R(k)/m_\pi$ converges to $k \cot \delta(k)/m_\pi$, which is real in this range of $k$. At Im $k > m_\pi/2$, while $k \cot \delta_R(k)/m_\pi$ at $R = 5$ fm agrees with the real part of $k \cot \delta(k)/m_\pi$, it gradually deviates from it as $R$ increases. Since $S(k, R)$ diverges as $R \to \infty$, $k \cot \delta_R(k)/m_\pi$ should approach to the bound state condition $-\sqrt{-(k/m_\pi)^2}$ (black dashed line) as $R \to \infty$. Such
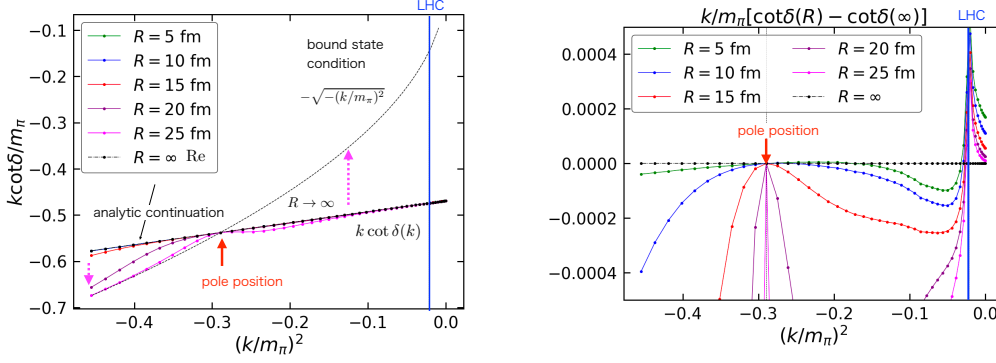
**Figure 2:** (Left) A comparison of $k \cot \delta(k)/m_\pi$ at $k^2 < 0$ region between the analytic continuation (black line, the real part only) and results with the IR cutoff, $R = 5$ fm(green), 10 fm(blue), 15 fm(red), 20 fm(violet) and 25 fm(magenta), together with the bound state condition $-\sqrt{-(k/m_\pi)^2}$ (black dashed line). (Right) A difference between $k \cot \delta_R(k)/m_\pi$ and the real part of $k \cot \delta(k)/m_\pi$.

behaviors observed in the left of the pole position, in particular, at $R = 25$ fm (magenta), while $k \cot \delta_R(k)/m_\pi$ is still close to the real part of $k \cot \delta(k)/m_\pi$ in the right of the pole position. This difference can be understood since the divergence is characterized by a factor $e^{(2\mathrm{Im}k - m_\pi)r'}$ in the integrand of Eq. (9). The larger Im $k$ is, the stronger the divergence factor becomes as $R$ increases.

Since $k_b(R)$ is almost $R$-independent in this range of $R$, we can easily estimate the correct value of the binding momentum $k_b$ from the $k \cot \delta_R(k)$ at finite but large $R$ without the $R \to \infty$ limit, even though $k \cot \delta_R(k)/m_\pi$ is different from $k \cot \delta(k)/m_\pi$ at Im $k > m_\pi/2$ other than $k_b$. While $S(k, R)$ is always real for pure imaginary $k$, $S_{\mathrm{anal}}(k)$ is complex for Im $k > m_\pi/2$.

In Fig. 2 (Right), a difference, $k \cot \delta_R(k) - \mathrm{Re}\,[k \cot \delta/m_\pi]$ are plotted. Properties mentioned above are more clearly seen. (1) $S(k, R)$ converges to $S_{\mathrm{anal}}(k)$ at Im $k < m_\pi/2$ as $R$ increases. (2) $S(k, R)$ deviates from $S_{\mathrm{anal}}(k)$ at Im $k > m_\pi/2$ except $k = k_b$. (3) The pole position of $S(k, R)$ reproduces the binding momentum $k_b$ correctly.

## 3. HAL QCD method with LHC

Based on knowledge obtained in the previous section, we discuss how we can treat the LHC in the HAL QCD method. Below we summarize the procedure to deal with the LHC in the HAL QCD method.

1. Since the potential is obtained in the HAL QCD method, we first investigate the long distance behavior of the potential. For example, the $D^*D$ potential in the $I = 0$ and $S$-wave channel, which is relevant for $T_{cc}^+$, is shown in Fig. 3 (Left). The 2-pion rather than 1-pion exchange has been observed at the long distance of the potential[6]. Thus the potential is fitted by 2-Gaussians + Yukawa$^2$,

$$V_{\mathrm{fit}}^{2\pi}(r; m_\pi) = \sum_{i=1}^{2} a_i e^{-r^2/b_i^2} + a_3 \left(1 - e^{-r^2/b_3^2}\right)^2 \left(\frac{e^{-m_\pi r}}{r}\right)^2, \tag{12}$$

as shown in the red band in the figure. Note that the 1-pion exchange, which is expected to exist, is not a dominant contribution in the $D^*D$ potential for $T_{cc}^+$.
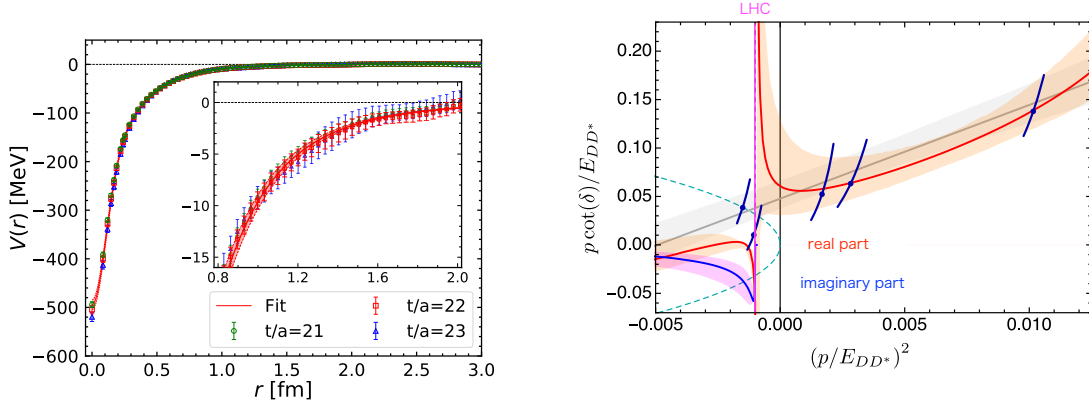
**Figure 3:** (Left) The $D^*D$ potential $V(r)$ in the $I = 0$ and $S$-wave channel as a function of $r$, obtained in lattice QCD at Euclidean time $t/a = 21$ (green circles), 22 (red squares) and 23 (blue triangles), together with the fit $V_{\text{fit}}^{2\pi}(r; m_\pi)$ to data at $t/a = 22$ (red band). This figure is taken from [6]. (Right) The reanalysis of $p \cot \delta(p)/E_{DD^*}$ data in [5] by including the effect of the LHC[7], where red and blue lines represent real and imaginary parts of $p \cot \delta(p)/E_{DD^*}$. We added few words in the figure taken from [7].

2. Next, we estimate positions of the LHC. For example, the LHC for the 2-pion exchange appears at

$$\frac{k_-^2}{m_\pi^2} \simeq \frac{(m_{D^*} - m_D)^2 - (2m_\pi)^2}{4m_\pi^2} \simeq -0.77, \tag{13}$$

while for the 1-pion exchange, it becomes

$$\frac{k_-^2}{m_\pi^2} \simeq \frac{(m_{D^*} - m_D)^2 - (m_\pi)^2}{4m_\pi^2} \simeq -0.02, \tag{14}$$

where $m_\pi = 146.4$ MeV, $m_D = 1878.2$ MeV and $m_{D^*} = 2018.1$ MeV in the simulation[6] are used.

3. We then compare the position of the LHC with the analytic continuation of $k \cot \delta(k)$. If a bound or virtual state appears above the branch point of the LHC, as seen in Fig. 1 (Left), the analysis by the analytic continuation is valid. If a bound state appears below the branch point of the LHC, we should directly extract the binding energy by solving the Schrödiner equation, rather than finding a crossing point between $k \cot \delta(k)$ and the bound state condition $-\sqrt{-k^2}$.

4. If a virtual state appears below the branch point of the LHC, the required analysis depends on the method to obtain data. In the case of the finite volume method, Fig. 3 (Right) shows an example of the analysis including the LHC[7], applied to finite volume spectra[5]. On the LHC, both real (red) and imaginary (blue) parts of $p \cot \delta(p)/E_{DD^*}$ appear, where $E_{DD^*} = \sqrt{p^2 + m_D^2} + \sqrt{p^2 + m_{D^*}^2}$, so that virtual pole on real $k^2$ claimed in [5] disappears. In the case of the HAL potential, however, the situation is different. Since the long distance behavior of the potential controls the position of the LHC, as discussed in the previous section, the analytic continuation knows the existence of the LHC, so that $k \cot \delta(k)$ automatically becomes complex on the LHC. Therefore, for example, in the case of $V_{\text{fit}}^{2\pi}(r; m_\pi)$ including

the 2-pion exchange, either virtual pole appears above the LHC of the 2-pion exchange at $k^2 \simeq -0.77 m_\pi^2$ or no virtual pole exists.

5. If the LHC is expected to exist, we may include it in the potential fit. For example, even though the 1-pion exchange contribution is not seen in the $D^*D$ potential, we may include it as an alternative fit to estimate its effects as

$$V_{\text{fit}}^{+1\pi}(r; m_\pi) = V_{\text{fit}}^{2\pi}(r; m_\pi) + a_4 \left(1 - e^{-r^2/b_4^2}\right) \frac{e^{-m_\pi r}}{r}. \tag{15}$$

The analysis with the alternative fit gives an estimate for systematic errors.

Note that the binding energy is not affected by the LHC, if the Schrödinger equation is directly solve. A difference between binding energies from $V_{\text{fit}}^{2\pi}(r; m_\pi)$ and $V_{\text{fit}}^{+1\pi}(r; m_\pi)$, if exists, is regarded as a systematic error, too.

## 4. Conclusion and discussion

The analysis using the non-relativistic potential shows that the analytic continuation and the result in the limit of the infra-red cutoff ($R \to \infty$) differ below the branch point of the LHC, except the binding momentum $k_b$. Thus the binding energy in the HAL QCD method is not affected by the LHC even if it exists. For the virtual state below the LHC, the analytic continuation can be performed through the HAL QCD potential in order to include an effect of the LHC. The long distance behavior which causes a particular type of the LHC may be included in the fit of the HAL QCD method, even if data show no such behavior. A doubly charmed tetra-quark state $T_{cc}^+$ in the previous HAL QCD method[6] appears as a virtual state above the branch point of the 1-pion LHC, and thus remains valid.

In order control the effect of the LHC, it is essential to determine the long distance behavior of the potential. Therefore the HAL QCD method is a more suitable framework than the finite volume method to do this explicitly.

## Acknowledgments

## References

[1] R. Aaij *et al.* [LHCb], *Observation of an exotic narrow doubly charmed tetraquark*, *Nature Phys.* **18** (2022) 751 [2109.01038].

[2] R. Aaij *et al.* [LHCb], *Study of the doubly charmed tetraquark $T_{cc}^+$*, *Nature Commun.* **13** (2022) 3351 [2109.01056].

[3] Y. Ikeda, B. Charron, S. Aoki, T. Doi, T. Hatsuda, T. Inoue, N. Ishii, K. Murano, H. Nemura and K. Sasaki, *Charmed tetraquarks $T_{cc}$ and $T_{cs}$ from dynamical lattice QCD simulations*, *Phys. Lett. B* **729** (2014) 85 [1311.6214].

[4] S. Chen, C. Shi, Y. Chen, M. Gong, Z. Liu, W. Sun and R. Zhang, *Tcc+(3875) relevant DD∗ scattering from Nf=2 lattice QCD*, *Phys. Lett. B* **833** (2022) 137391 [2206.06185].

[5] M. Padmanath and S. Prelovsek, *Signature of a Doubly Charm Tetraquark Pole in DD\* Scattering on the Lattice*, *Phys. Rev. Lett.* **129** (2022) 032002 [2202.10110].

[6] Y. Lyu, S. Aoki, T. Doi, T. Hatsuda, Y. Ikeda and J. Meng, *Doubly Charmed Tetraquark Tcc+ from Lattice QCD near Physical Point*, *Phys. Rev. Lett.* **131** (2023) 161901 [2302.04505].

[7] M. L. Du, A. Filin, V. Baru, X. K. Dong, E. Epelbaum, F. K. Guo, C. Hanhart, A. Nefediev, J. Nieves and Q. Wang, *Role of Left-Hand Cut Contributions on Pole Extractions from Lattice Data: Case Study for Tcc(3875)+*, *Phys. Rev. Lett.* **131** (2023) 131903 [2303.09441].

[8] L. Meng, V. Baru, E. Epelbaum, A. A. Filin and A. M. Gasparyan, *Solving the left-hand cut problem in lattice QCD: Tcc(3875)+ from finite volume energy levels*, *Phys. Rev. D* **109** (2024) L071506 [2312.01930].

[9] S. Collins, A. Nefediev, M. Padmanath and S. Prelovsek, *Toward the quark mass dependence of Tcc+ from lattice QCD*, *Phys. Rev. D* **109** (2024) 094509 [2402.14715].

[10] A. B. Raposo and M. T. Hansen, *Finite-volume scattering on the left-hand cut*, *JHEP* **08** (2024) 075 [2311.18793].